Inorg. Chem. **2002**, *41*, 5479–5486

$Gd_{1.33}Pt_3(Al,Si)_8$ and $Gd_{0.67}Pt_2(Al,Si)_5$: Two Structures Containing a Disordered Gd/Al Layer Grown in Liquid Aluminum

S. E. Latturner and M. G. Kanatzidis*

Department of Chemistry, Michigan State University, East Lansing, Michigan 48824

Received March 29, 2002

$Gd_{1.33}Pt_3Al_8$ was synthesized by the combination of Gd and Pt in excess liquid aluminum. Addition of silicon resulted in the incorporation of a small amount of this element into the material to form the isostructural $Gd_{1.33}Pt_3Al_7Si$. Both compounds grow as rodlike crystals with hexagonal cross section. The structures were refined in the rhombohedral space group $R\bar{3}m$, with cell parameters $a = 4.3359(6)$ Å and $c = 38.702(8)$ Å for the ternary and $a = 4.3280(8)$ Å and $c = 38.62(1)$ Å for the quaternary compound. The structure is comprised of stuffed arsenic-like $PtAl_2$ layers and disordered Gd/Al layers. Analysis of the *hk*0 zone reflections indicate the presence of an $a^* = \sqrt{3}a$ supercell, but the structure is not ordered along *c*, as revealed by the highly diffuse reflections in the 0*kl* zone photos. Therefore, the compounds are disordered variants of the $Gd_4Pt_9Al_{24}$ type. Magnetic susceptibility studies reveal antiferromagnetic transitions at 15 K for the ternary and 7 K for the quaternary compound. Variation of the reactant ratio produces a different structure comprised of the same structural blocks, including the disordered Gd/Al layer. $Gd_{0.67}Pt_2Al_5$ and its quaternary analogue $Gd_{0.67}Pt_2Al_4Si$ form in the hexagonal system $P6_3/mmc$ with cell parameters $a = 4.2907(3)$ Å and $c = 16.388(2)$ Å for the ternary and $a = 4.2485(6)$ Å and $c = 16.156(3)$ Å for the quaternary compound.

Introduction

Synthesis in a flux medium offers a great advantage in growing high-quality crystals of a number of compounds. Large crystals of refractory borides such as TiB_2, VB_2, and LaB_6 can be grown from aluminum flux.[1] Gallium nitride can be grown from the combination of gallium metal and NaN_3; heating this mixture causes the azide to decompose to nitrogen (the source of nitrogen for GaN) and sodium (which acts as the flux for crystal growth).[2] Flux growth has also allowed for the determination of crystal structures of refractory compounds previously only isolable as powders via the standard high-temperature synthesis routes. For instance, gallium flux was used to grow large crystals of $YNiSi_3$, which allowed the structure and properties of this compound to be determined.[3]

Low melting fluxes are even more useful in exploratory synthesis. A number of new compounds with complex stoichiometries have been discovered recently by combining a rare earth element, a late transition metal, and a group 14 element in liquid aluminum or gallium. With nickel alone, a plethora of new structures have resulted, such as $RENiAl_4Ge_2$,[4] $RE_2Ni(Ni_xSi_{1-x})Al_4Si_6$,[5] $RE_{0.67}Ni_2Ga_4Ge$[6] (RE = rare earth), and the aforementioned $YNiSi_3$.[3] The flux acts as a solvent to a wide range of reactants, particularly for group 14 elements silicon and germanium, which are rendered active at temperatures well below their normal melting points. Lower temperatures generally facilitate the formation of kinetically derived materials that may not be accessible by traditional high-temperature synthetic methods such as arc melting or rf heating. Even within the flux growth scenario, variation of the reaction time and temperature can influence the product outcome within a system.

* To whom correspondence should be addressed. E-mail: kanatzid@cem.msu.edu.

(1) a) Canfield, P. C.; Fisk, Z. *Philos. Mag. B* **1992**, *65*, 1117−1123. (b) Otani, S.; Ohsawa, T. *J. Cryst. Growth* **1999**, *200*, 472−475. (c) Okada, S.; Atoda, T.; Higashi, I.; Takahashi, Y. *J. Chem. Soc. Jpn.* **1985**, 1.

(2) Yamane, H.; Kinno, D.; Shimada, M.; Sekiguchi, T.; DiSalvo, F. J. *J. Mater. Sci.* **2000**, *35*, 801−808.

(3) Chen, X. Z.; Larson, P.; Sportouch, S.; Brazis, P.; Mahanti, S. D.; Kannewurf, C. R.; Kanatzidis, M. G. *Chem. Mater.* **1999**, *11*, 75−83.

(4) Sieve, B.; Chen, X.; Cowen, J.; Larson, P.; Mahanti, S. D.; Kanatzidis, M. G. *Chem. Mater.* **1999**, *11*, 2451−2455.

(5) Chen, X. Z.; Sportouch, S.; Sieve, B.; Brazis, P.; Kannewurf, C. R.; Cowen, J. A.; Patschke, R.; Kanatzidis, M. G. *Chem. Mater.* **1998**, *10*, 3202−3211.

(6) Zhuravleva, M.; Chen, X. Z.; Wang, X.; Schultz, A. J.; Ireland, J.; Kannewurf, C. K.; Kanatzidis, M. G. *Chem. Mater.* **2002**, *14*, 3066−3081.

10.1021/ic025623n CCC: $22.00
Published on Web 09/26/2002

Table 1. Crystallographic Data and Structural Refinement Parameters for $Gd_{1.33}Pt_3Al_8$, $Gd_{1.33}Pt_{3.0}Al_{6.7}Si_{1.0}$, $Gd_{0.67}Pt_2Al_5$, and $Gd_{0.67}Pt_2Al_4Si$

	$Gd_{1.33}Pt_3Al_8$	$Gd_{1.33}Pt_3Al_7Si$	$Gd_{0.67}Pt_2Al_5$	$Gd_{0.67}Pt_2Al_4Si$
fw	1010.26	1011.37	630.45	631.55
space group	$R\bar{3}m$	$R\bar{3}m$	$P6_3/mmc$	$P6_3/mmc$
a (Å)	4.3359(6)	4.3280(8)	4.2907(3)	4.2482(6)
c (Å)	38.702(8)	38.62(1)	16.388(2)	16.156(3)
V (Å^3)	630.12	626.52	261.28	252.51
Z	3	3	2	2
d_{calc} (g/cm^3)	7.987	8.042	8.014	8.307
temp (°C)	25	25	25	25
radiation	Mo Kα	Mo Kα	Mo Kα	Mo Kα
μ (mm^{-1})	38.82	19.53	33.32	32.31
R1/wR2 [$I > 2\sigma(I)$][a]	0.0208/0.0476	0.0351/0.0903	0.0231/0.0551	0.0300/0.0693
R1/wR2 (all data)	0.0245/0.0487	0.0377/0.0913	0.0271/0.0565	0.0309/0.0700

[a] $R1 = \Sigma||F_o| - |F_c||/\Sigma|F_o|$; $wR2 = [\Sigma w\{|F_o| - |F_c|\}^2/\Sigma w|F_o|^2]^{1/2}$, $w = 1/\sigma^2\{|F_o|\}$.

Our exploration of complex intermetallics grown from liquid aluminum and gallium has recently been extended to incorporate the third row transition metals. Syntheses using gold have resulted in a number of new phases such as the $Th_2(Au_xSi_{1-x})[AuAl_2]_nSi_2$ series, characterized by the presence of $AuAl_2$ slabs of varying widths.[7] Platinum is being investigated for comparison and in anticipation of a similar broad range of new structures. Platinum intermetallics are also of interest for use as catalysts[8] and for high-temperature applications such as inert coatings for titanium alloys.[9] Here we report the structural and magnetic properties of four Gd/Pt/(Al,Si) intermetallic compounds grown from liquid aluminum. Their structure features platinum atoms in a stuffed arsenic type coordination environment and a monatomic plane of rare earth ions and triangles of aluminum atoms which exhibits extensive stacking disorder. In the $Gd_{1.33}Pt_3(Al,Si)_8$ structure, this disorder results in a higher apparent symmetry than is present in the recently reported ordered archetype $Gd_4Pt_9Al_{24}$, which is comprised of the same building blocks.[10] The relationship between these compounds will be discussed.

Experimental Procedure

Synthesis. In a nitrogen-filled glovebox, Gd (Cerac, 99.9%), Pt powder (Alfa-Aesar, 99.95%), Al pellets (Cerac, 99.99%), and Si (Cerac, 99.9%) were combined in a 1:1:10:5 molar ratio in an alumina crucible. This was placed into a fused silica tube which was sealed under a vacuum of 10^{-4} Torr. This sample was then heated to 1000 °C in 12 h, held at this temperature for 15 h, cooled to 860 °C in 1 day, annealed at 860 °C for 2 days, and slowly cooled to room temperature over 3 days. The aluminum flux was removed by soaking the crucible in 5 M NaOH for 1 day. Single crystals were selected from the product for elemental analysis, X-ray diffraction, and magnetic susceptibility measurements. The yield of $Gd_{1.33}Pt_3Al_7Si$ was very low (10%, based on rare earth), so additional syntheses were explored in an attempt to increase the yield. A synthesis carried out without silicon (Gd:Pt:Al ratio 1:1:12) yielded a ternary version of the compound, $Gd_{1.33}Pt_3Al_8$, in 12% yield based on Gd. A Gd/Pt/Al/Si reactant ratio of 0.33:1:10:5, prepared in the same manner, produced $Gd_{0.67}Pt_2Al_4Si$, a different quaternary compound, in 20% yield based on Gd. Omitting the silicon in this reaction (Gd:Pt:Al ratio 0.33:1:12) resulted in the ternary version $Gd_{0.67}Pt_2Al_5$, in 25% yield based on Gd. The majority product in all three syntheses was $GdAl_3$.

EDS Analysis. Selected single crystals were affixed to an SEM plate using carbon tape. Microprobe analysis of these samples was performed using a JEOL JSM-35C scanning electron microscope equipped with a Tracor Northern energy dispersive spectroscopy (EDS) detector. Data were acquired using a 20 kV accelerating voltage and an accumulation time of 50 s. The elemental ratios in the approximately 60 analyzed crystals from the 1:1:12 and 0.33:1:12 ternary reactions were very consistent, with average compositions of $GdPt_3Al_7$ and $GdPt_2Al_5$, respectively. Crystals isolated from the quaternary reactions were found to have elemental ratios of $GdPt_3Al_6Si$ (from the 1:1:10:5 reactant mixture) and $GdPt_2Al_4Si$ (from the 0.33:1:10:5 synthesis). The Gd:Pt:(Al + Si) ratios observed for all the products are in fair agreement with the results obtained from the X-ray refinement (vide infra), the only discrepancy being slightly low aluminum readings.

X-ray Crystallography. Full-sphere single-crystal X-ray diffraction data for the ternary and quaternary compounds were collected at room temperature on a Bruker AXS SMART CCD diffractometer. Data processing was then performed using the program SAINT; an absorption correction was applied to the data using the SADABS program.[11] The structure was solved using direct methods and refined with the SHELXTL package of programs.[12] The crystallographic and refinement data are listed in Tables 1−5. The aluminum and silicon atoms in the quaternary materials could not be distinguished in the X-ray refinement due to their similar number of electrons. Bond length analysis also proved inconclusive, indicating that silicon might be substituting in small amounts on all aluminum sites (vide infra). The refinements were therefore carried out using aluminum on all the possible mixed sites. Bond lengths and angles are shown in Table 6. X-ray photographs of the *hk*0 and 0*kl* zones were collected on multiple crystals of the $Gd_{1.33}Pt_3(Al,Si)_8$ compounds with 3000 s exposures.

Magnetic Susceptibility Measurements. Magnetic susceptibility measurements were carried out with a Quantum Design SQUID magnetometer at temperatures between 2 and 300 K. For isotropic data, selected crystals were ground into powder and placed into a polypropylene sample holder. Field-cooled and zero-field-cooled

(7) Latturner, S. E.; Bilc, D.; Mahanti, S. D.; Kanatzidis, M. G. *Chem. Mater*. **2002**, *14*, 1695−1705.
(8) Komatsu, T.; Mesuda, M.; Yashima, T. *Appl. Catal., A* **2000**, *194*, 333−339.
(9) Gurrappa, I.; Gogia, A. K. *Surf. Coat. Technol*. **2001**, *139*, 216−221.
(10) Thiede, V.; Fehrmann, B.; Jeitschko, W. *Z. Anorg. Allg. Chem*. **1999**, *625*, 1417−1425.
(11) *SAINT*, version 4; Siemens Analytical X-ray Instruments, Inc.: Madison, WI, 1995. *SADABS*, University of Göttingen: Göttingen, Germany.
(12) Sheldrick, G. M. *SHELXTL. Structure Determination Programs*, version 5.0; Siemens Analytical X-ray Instruments, Inc.: Madison, WI, 1995

Table 2. Atomic Positions and Equivalent Isotropic Displacement Parameters (Å^2) for $Gd_{1.33}Pt_3Al_8$

atom	site	x	y	z	U_{eq}[a]	occ
Gd	6*c*	0	0	0.26936(3)	0.0059(4)	0.670(4)
Pt(1)	3*a*	0	0	0	0.0054(3)	1
Pt(2)	6*c*	0	0	0.12071(1)	0.0060(2)	1
Al(1)	6*c*	0	0	0.4442(1)	0.0074(9)	1
Al(2)	6*c*	0	0	0.1865(1)	0.0073(9)	1
Al(3)	6*c*	0	0	0.3507(1)	0.0081(9)	1
Al(4)	18*h*	0.540(1)	0.460(1)	0.3947(2)	0.010(3)	0.35(1)

[a] In this and subsequent tables, U_{eq} is defined as one-third of the trace of the orthogonalized $\mathbf{U}_{ij}$ tensor.

Table 3. Atomic Positions and Equivalent Isotropic Displacement Parameters (Å^2) for $Gd_{1.33}Pt_{3.0}Al_{6.7}Si_{1.0}$

atom	site	x	y	z	U_{eq}	occ
Gd	6*c*	0	0	0.26938(5)	0.0054(8)	0.624(7)
Pt(1)	3*a*	0	0	0	0.0077(5)	1
Pt(2)	6*c*	0	0	0.12077(2)	0.0087(5)	1
Al(1)	6*c*	0	0	0.4438(2)	0.011(2)	1
Al(2)	6*c*	0	0	0.1864(2)	0.011(2)	1
Al(3)	6*c*	0	0	0.3511(2)	0.009(2)	1
Al(4)	18*h*	0.540(2)	0.460(2)	0.3947(3)	0.008(5)	0.29(2)

Table 4. Atomic Positions and Equivalent Isotropic Displacement Parameters (Å^2) for $Gd_{0.67}Pt_2Al_5$

atom	site	x	y	z	U_{eq}	occ
Gd	2*c*	1/3	2/3	1/4	0.0064(3)	0.690(6)
Pt(1)	4*f*	1/3	2/3	0.60832(2)	0.0061(2)	1
Al(1)	4*e*	0	0	0.1345(2)	0.0070(5)	1
Al(2)	4*f*	1/3	2/3	0.0464(2)	0.0072(5)	1
Al(3)	6*h*	0.539(1)	0.077(2)	1/4	0.010(2)	0.37(2)

Table 5. Atomic Positions and Equivalent Isotropic Displacement Parameters (Å^2) for $Gd_{0.67}Pt_2Al_4Si$

atom	site	x	y	z	U_{eq}	occ
Gd	2*c*	1/3	2/3	1/4	0.0095(9)	0.525(6)
Pt(1)	4*f*	1/3	2/3	0.61015(4)	0.0104(4)	1
Al(1)	4*e*	0	0	0.1382(3)	0.013(1)	1
Al(2)	4*f*	1/3	2/3	0.0479(3)	0.009(1)	1
Al(3)	6*h*	0.530(1)	0.061(3)	1/4	0.015(4)	0.32(2)

Table 6. Selected Bond Lengths (Å)

	$Gd_{1.33}Pt_3Al_8$	$Gd_{1.33}Pt_3Al_7Si$		$Gd_{0.67}Pt_2Al_5$	$Gd_{0.67}Pt_2Al_4Si$
Pt(1)−Al(4)	2.560(8)	2.55(1)			
Pt(1)−Al(3)	2.592(1)	2.591(2)			
Pt(2)−Al(4)	2.485(7)	2.48(1)	Pt−Al(3)	2.509(3)	2.472(4)
Pt(2)−Al(1)	2.5319(8)	2.530(2)	Pt−Al(1)	2.5141(5)	2.4941(9)
Pt(2)−Al(2)	2.546(5)	2.534(8)	Pt−Al(2)	2.536(3)	2.554(6)
	2.700(2)	2.696(3)		2.677(1)	2.651(2)
Gd−Pt(2)	3.3301(8)	3.325(1)	Gd−Pt	3.3953(3)	3.3348(6)
Gd−Al(4)	1.556(7)[a]	1.55(1)[a]	Gd−Al(3)	1.525(8)[a]	1.45(1)[a]
	3.092(5)	3.09(1)		3.066(6)	3.079(7)
Gd−Al(3)	3.085(3)	3.071(5)	Gd−Al(1)	3.118(2)	3.046(3)
Gd−Al(1)	3.092(3)	3.077(5)	Gd−Al(2)	3.336(3)	3.265(6)
Al(4)−Al(4)	1.65(1)[a]	1.64(3)[a]	Al(3)−Al(3)	1.65(1)[a]	1.74(2)[a]
	2.69(1)	2.69(3)		2.64(1)	2.51(2)

[a] These unreasonable interatomic distances are between partially occupied sites, as explained in the text.

data were collected at 500 G. To determine the anisotropic characteristics of the magnetic behavior, rod-shaped single crystals of $Gd_{1.33}Pt_3(Al,Si)_8$ were aligned along their *c*-axis between layers of Kapton tape. FC and ZFC data sets were collected at 500 G with the *c*-axis aligned parallel and perpendicular to the magnetic field of the SQUID. Field dependence data was also collected at 3 K for both the powder and crystal samples.

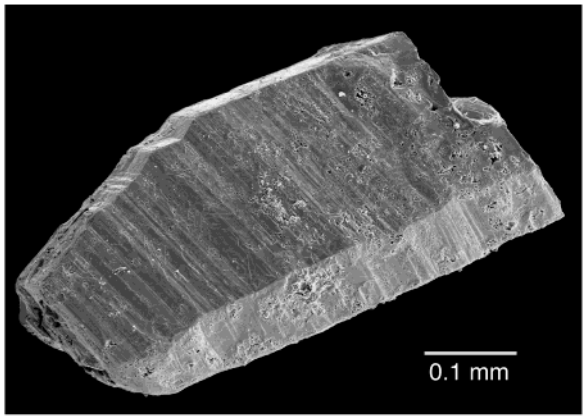

Figure 1. Representative crystal of $Gd_{1.33}Pt_3Al_7Si$, showing rodlike morphology and hexagonal cross section. Note the striations on the [100] and [010] faces resulting in a corrugated surface.

Results and Discussion

$Gd_{1.33}Pt_3Al_8$ and $Gd_{1.33}Pt_3Al_7Si$ crystallize as metallic-looking faceted hexagonal rods which can reach up to 1 mm in length and 0.4 mm in width. Some of the rods are tapered at one end, forming a pencil shape, as seen in Figure 1. The rods also appear to have corrugated surfaces; the corrugation lines are perpendicular to the rod's long direction, probably indicative of stacking faults in the crystals along the *c*-axis (additional support for this hypothesis is discussed below). $Gd_{0.67}Pt_2Al_5$ and $Gd_{0.67}Pt_2Al_4Si$ also form as hexagonal rods, but they are not characterized by the aforementioned uneven surfaces. These ternary and quaternary intermetallics only account for 10−20% of the solid isolated after removal of the flux. The remaining product consists predominantly of $GdAl_3$ needles but also contains platelike silicon crystals and crystals of $GdAl_2Si_2$. Attempts to incorporate a higher amount of silicon into the quaternary structures failed, resulting instead in more recrystallized silicon as a byproduct.

Structure Description. The crystal structure of $Gd_{1.33}Pt_3(Al, Si)_8$ is shown in Figure 2. This material adopts a disordered modification of the structure of $RE_4Pt_9Al_{24}$ (RE = late rare earth; vide infra).[10] The latter was described as triclinic ($P\bar{1}$), but $Gd_{1.33}Pt_3(Al, Si)_8$ was found to crystallize in rhombohedral space group $R\bar{3}m$. This structure can be described as a stacking of three types of layers in a sequence ABCBA′BC′BA″BC″B, where A is a Pt_2Al_4 double layer, B is a disordered Gd/Al layer, and C is a $PtAl_2$ single layer; see Figures 3 and 4. The positioning of the layers with respect to each other is indicated by A′, A″, etc.; as discussed in the next sections, the staggering of the Gd/Al layer is not ordered. $Gd_{0.67}Pt_2(Al,Si)_5$ can be described in hexagonal space group $P6_3/mmc$ and is analogous to the new quaternary phases $RE_{0.67}Ni_2Ga_{5-x}Ge_x$ recently isolated from gallium flux.[6] The structure of $Gd_{0.67}Pt_2(Al,Si)_5$ is comprised of two of the building blocks found in the rhombohedral phase—alternating Pt_2Al_4 double layers and Gd/Al disordered layers, as seen in Figure 5. The platinum atoms have similar coordination environments in both these structures; the Pt_2Al_4 slab can be viewed as a linked pair of two $PtAl_2$ layers.

$PtAl_2$ Single Layer and Pt_2Al_4 Double Layer. The $PtAl_2$ slab, shown in Figure 3a, is comprised of a triangular net of

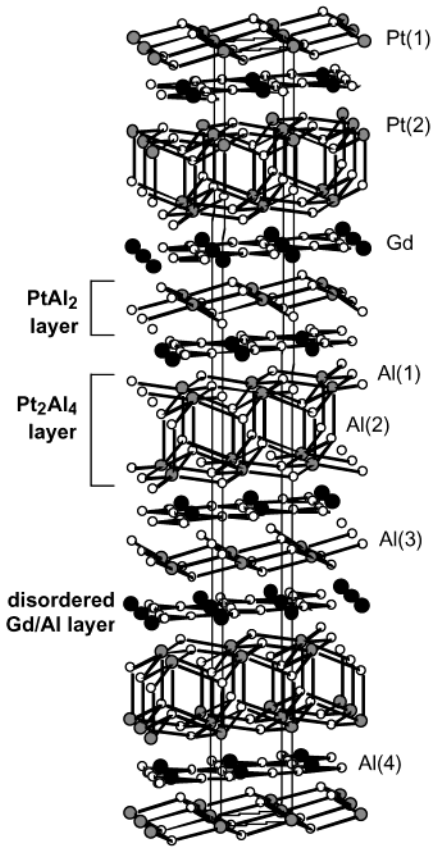

Figure 2. Structure of $Gd_{1.33}Pt_3Al_8$ shown as a stacking of layers for clarity. The absence of drawn bonds between layers is for illustrative purposes only and does not imply that bonding is weak or absent between the layers.

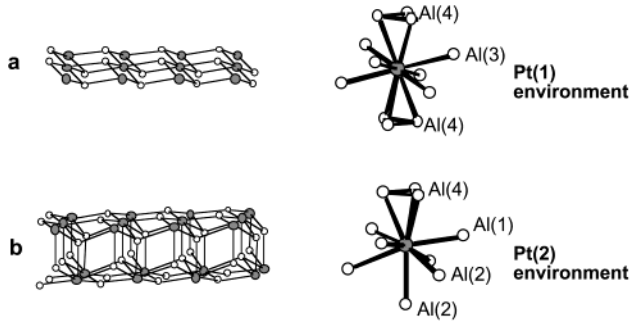

Figure 3. Structural motifs found in the compounds discussed in this work: (a) the $PtAl_2$ slab, showing the local environment of the Pt(1) atom in this layer; (b) the Pt_2Al_4 slab and the local environment of the Pt(2) atom in this layer.

platinum atoms sandwiched between two similar nets of aluminum atoms. This is the same kind of layer found in $Y_2Co_3Ga_9$ and its aluminum analogues[13] and in $SmNiAl_4Ge_2$.[4] The triangles of aluminum atoms above and below each platinum atom create a highly distorted octahedral environment (severely compressed along the 3-fold axis) for the platinum in this layer. This can also be described as a "stuffed" arsenic type slab, with puckered cyclohexane-like rings centered by a platinum atom. The Al−Al distances are 2.85(5) Å, whereas the Pt−Al distances are 2.591(2) Å. The

(13) (a) Grin', Y. N.; Gladyshevskii, R. E.; Sichevich, O. M.; Zavodnik, V. E.; Yarmolyuk, Y. P.; Rozhdestvenskaya, I. V. *Sov. Phys. Crystallogr.* **1984**, *29*, 528−530. (b) Gladyshevskii, R. E.; Cenzual, K.; Parthe, E. *J. Alloys Compd.* **1992**, *182*, 165−170.

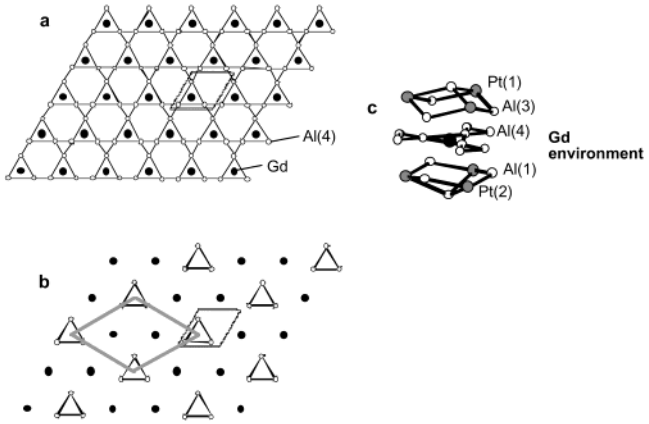

Figure 4. Disordered rare earth−aluminum layer found in the compounds discussed in this work: (a) the Gd/Al layer with both sites fully occupied, viewed down the *c*-axis, where the 4.3 Å cell is indicated; (b) the superstructure in the *ab*-plane that results from the partial occupancy of the Gd and Al sites in this layer, where the 7.5 Å supercell is indicated in gray; (c) local environment of Gd in this layer, viewed down the *a*-axis.

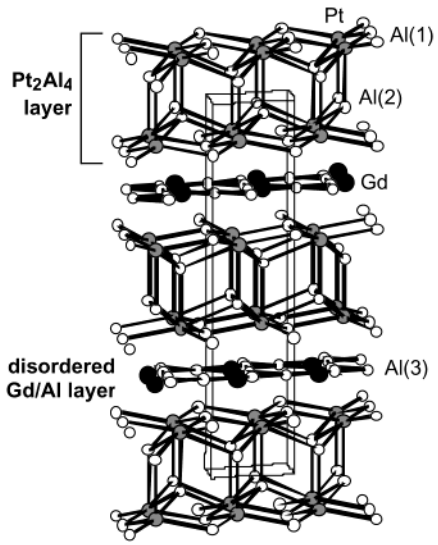

Figure 5. Structure of $Gd_{0.67}Pt_2Al_5$. Bonds between the Gd/Al layer and the Pt_2Al_4 layer have been omitted for clarity.

platinum atoms in this layer are also bonded to Al atoms above and below the $PtAl_2$ slab at a distance of 2.56(1) Å.

The Pt_2Al_4 double layer is essentially a pair of $PtAl_2$ single layers staggered and linked through Pt−Al bonds. This results in a layer of 5.5 Å thickness, compared to the 2.6 Å of the single $PtAl_2$ layer. The platinum atoms in the single $PtAl_2$ layer are perfectly centered between the aluminum sheets; in the double Pt_2Al_4 slab, the platinum atoms are pushed toward the capping Al(1) layer, resulting in a very asymmetrical environment shown in Figure 3b.

Disordered Gd/Al Layer. This monatomic layer has similar characteristics in all four structures studied in this work. Understanding the disordered configuration of this layer is key to comprehending the full structure of these compounds. The Gd atoms are situated in a triangular net with 4.3 Å between neighboring sites. The electron density at this site indicated less than complete occupancy, and there was significant residual density in the plane in locations between the Gd triangles. Putting this density into the model as aluminum atoms resulted in a large drop in the R-value.

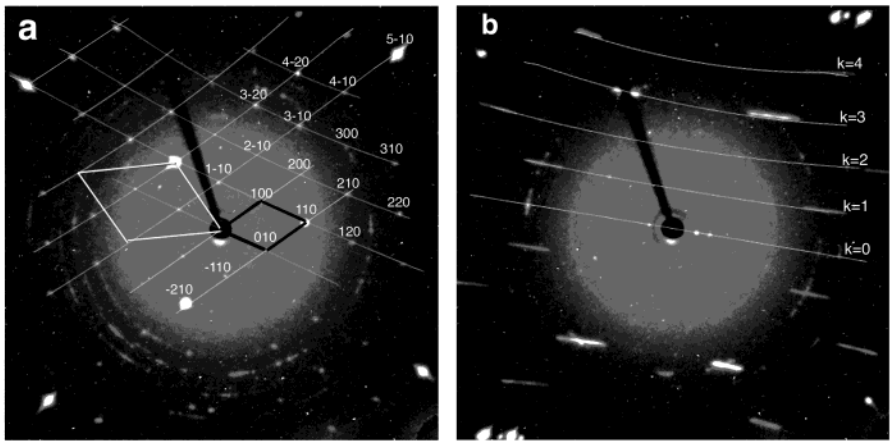

Figure 6. Zone photographs for $Gd_{1.33}Pt_3Al_7Si$: (a) the *hk*0 zone photo, which can be indexed on a 7.5 Å supercell ($\sqrt{3}a$) in the *ab*-plane; (b) the *h*0*l* zone, indicating disorder in the stacking of the various planes along the *c*-axis.

As shown in Figure 4a, the resulting structure is the same triangular net, comprised now of $GdAl_3$ units. This arrangement possesses unrealistically short Gd−Al and Al−Al distances of 1.45−1.55 and 1.65−1.75 Å, respectively (see the highlighted entries in Table 6). Furthermore, partial occupancies of approximately 66% and 33% were observed for both the Gd and Al atoms in this layer. This phenomenon is a classic symptom of observing an averaged structure through a subcell. In other words, the disordered $GdAl_3$ layer of Figure 4a is a "collapsed" structure, likely an artifact, deriving from the fact that a larger cell is needed to describe this part of the structure. A supercell with a cell edge of $\sqrt{3}a \times \sqrt{3}a$ (i.e. 7.5 × 7.5 Å) could explain both the structural motif of Figure 4a and the observed occupancies. Despite this realization we were not able to index the collected diffraction data to larger cells than the ones we report here.

This hexagonal $REAl_3$ layer appears to have exceptional stability and has been observed in a number of ternary and quaternary intermetallic compounds. Gladyshevskii et al. characterized a family of $RENi_3Al_9$ ternary structures which had either ordered arrangements of rare earth atoms and aluminum triangles (for RE = Er and Gd) or partially disordered arrangements of these moieties (for RE = Y and Dy).[14] Favorable comparison of the Al−Al distances in the Al triangles of $Gd_{1.33}Pt_3Al_7Si$ (2.69(3) Å) with those observed in RNi_3Al_9 (2.64 Å) indicates that silicon is likely not substituting on this site. This distance in the other quaternary compound studied here ($Gd_{0.67}Pt_2Al_4Si$) is significantly shorter at 2.51(2) Å and may indicate the presence of silicon at this site. Si−Si bonds in intermetallics often fall in the 2.35−2.45 Å range; Al−Al bonds are usually over 2.6 Å in length. An intermediate distance of 2.51 Å is reasonable for an Al−Si bond, supporting the possibility of Si substitution in the triangles. This is in contrast to the results of neutron diffraction studies of the gallium and germanium distribution in the isostructural $Y_{0.67}Ni_2Ga_{5-x}Ge_x$, which indicate that gallium and not the tetrelide element preferentially occupies the corresponding triangular sites.[6]

(14) Gladyshevskii, R. E.; Cenzual, K.; Flack, H. D.; Parthe, E. *Acta Crystallogr.* **1993**, *B49*, 468−474.

Zone photographs of crystals of $Gd_{1.33}Pt_3Al_7Si$ were taken to investigate the extent of the Gd/Al layer ordering in the compounds studied here. Short *hk*0 zone acquisition times (less than 600 s) reveal only the seven bright spots in Figure 6a. These can be indexed on a 4.3 Å unit cell, outlined in white in the figure. However, considerably longer collection times (3000 s) reveal weak superstructure reflections in a hexagonal pattern, corresponding to the presence of a 7.5 Å cell which is a $\sqrt{3}a$ supercell of the $R\bar{3}m$ structure. These weak reflections are not present in the full sphere data due to the short exposure times (15 s) used. The supercell and the indexing based on it are shown in the figure. The experimental observation of the supercell strongly supports the ordering model proposed in Figure 4b.

The 0*kl* zone photograph in Figure 6b is also highly informative; it indicates that the supercell is not ordered along the *c*-axis of the structure. Instead of sharp Bragg peaks, the reflections along the *c**-axis are predominantly faint broad streaks. This streaking strongly indicates considerable disorder associated with the stacking of layers along the *c*-axis. The few sharp reflections in this zone photo can be indexed to the 38 Å repeat unit found in our data collection and used in structure refinement. This repeat distance is due to the staggering order of the $PtAl_2$ and Pt_2Al_4 layers. Indexing along the *k* direction reveals a *b*-axis parameter of 7.5 Å, in agreement with the results of the *hk*0 zone photograph.

Jeitschko et al. recently reported the structure of a series of compounds $RE_4Pt_9Al_{24}$ with RE = late rare earth metals.[10] These materials are comprised of identical layers as the $Gd_{1.33}Pt_3(Al,Si)_8$ compounds discussed here, but the rare earth−aluminum layers are ordered. The nature of this ordering varies with the rare earth. For $Er_4Pt_9Al_{24}$, the Er/Al layer is ordered not only within the layer but also in its positioning with respect to the other layers in the unit cell (i.e., it has an ordered staggering arrangement). This destroys the 3-fold rotational symmetry, because while each kind of layer in the compound possesses a 3-fold axis, these axes do not coincide with each other. The result is a $P\bar{1}$ triclinic cell, albeit with *a*- and *b*-cell edges that are very similar and a γ angle close to 60° (a = 7.461 Å, b = 7.462 Å, c = 13.044 Å; α = 90.00°, β = 100.94°, γ = 60.13°). For Y_4-

Pt_9Al_{24}, on the other hand, this ordering is not complete. Analysis of the refinement results using the same triclinic cell indicated the presence of residual electron density in the Y/Al layer corresponding to misplaced layers (with their atoms being shifted by ±[1/3,1/3] in the *ab*-plane). When these out-of-register sites were included in the refinement, their low occupancies (<20%) indicated a fairly small amount of disorder in the stacking and orientation of the layers.[10]

Each slab extending in the *ab*-plane in the $Gd_{1.33}Pt_3(Al,Si)_8$ structure (and by similar reasoning, the $Gd_{0.67}Pt_2(Al,Si)_5$ structure) is ordered. The stacking and registry however of the $PtAl_2$ and Pt_2Al_4 slabs with respect to the Gd/Al monatomic layers—which possesses a 7.5 Å × 7.5 Å ordered configuration in the *ab*-plane—is not. The lack of registry of the slabs along *c* renders the structure unable to develop a stable and coherent lattice *c*-constant. Thus, the reciprocal lattice points along *c** become extremely large, i.e., diffuse, as seen in the 0*kl* zone photos which show streaks instead of distinct reflections along the *l* direction. All this however does not affect the superstructure in the *ab*-plane which is apparent in the *hk*0 zone photos. It is this lack of order that makes it appropriate to use the structural formula $Gd_{1.33}Pt_3Al_8$ to emphasize that this compound is a disordered, averaged subcell of the ordered parent compound $Gd_4Pt_9Al_{24}$.

The disorder in the positioning of the Gd/Al planes in $Gd_{1.33}Pt_3Al_8$ is likely the result of the short reaction times that were used in this study. During synthesis, these compounds were annealed at 860 °C for only 2 days. While the more ordered compounds studied by Jeitschko et al. were also grown from aluminum flux, a much longer annealing time (300 h at 850 °C) was used. Promotion of ordering by long heating times is a relatively commonly observed phenomenon. Recent studies on $GdNi_{5-x}Tr_x$ (Tr = Al, Ga, In), a family of intermetallic compounds of interest for hydrogen storage, have shown that the crystal structure of some of the materials is very dependent on heat treatment.[15] While as-cast alloys of $GdNi_3Ga_2$ crystallize in the $CaCu_5$ structure type, lengthy annealing times result in an ordering of the nickel and gallium to form a superstructure of the YCo_3Ga_2 type.

A survey of the published structures with similar layers of rare earth ions and triangles of aluminum (or gallium) also indicates the importance of reaction conditions in promoting ordering. Aluminide analogues of the $Y_2Co_3Ga_9$ structure have been synthesized with a variety of rare earth and transition metals; examples include $Ce_2Ir_3Al_9$ and $Ce_2Rh_3Al_9$.[13,16]This structure consists of the stuffed arsenic type slab (see the $PtAl_2$ layer, Figure 3a) alternating with the $REAl_3$ triangle layer. In all published accounts of these compounds, arc melting followed by lengthy (5 or more days) annealing at high temperatures was used as the synthetic technique, and the $REAl_3$ layer is ordered. $RENi_3Al_9$ also contains this layer, alternating with a Ni_2Al_5 slab that can be related to the Pt_2Al_4 layer described herein (shown in Figure 3b) by the addition of another layer of Al atoms. Four analogues of this structure were synthesized by arc melting, followed by annealing at 1073 K for 2 weeks.[14] The Gd and Er compounds were found to have no disorder in the RE/Al triangle layer. The Y and Dy analogues had partial disorder corresponding to the presence of some RE/Al layers being shifted out of alignment along a specific vector, similar to the situation described for $Y_4Pt_9Al_{24}$. However, it was noted that a structure with maximum disorder in this layer would result in an averaged higher symmetry, changing the space group from *R*32 to $P\bar{6}m2$. This kind of disorder was not observed.[14] It appears that the higher temperatures afforded by arc melting and high temperature annealing promote the formation of the thermodynamically favored ordered arrangement of $REAl_3$ triangle layers, as the lengthy annealing time did in the Al flux growth of $RE_4Pt_9Al_{24}$. Experiments are currently underway to investigate the effects of longer annealing times on the disordered $Gd_{1.33}Pt_3Al_8$ materials synthesized in this work.

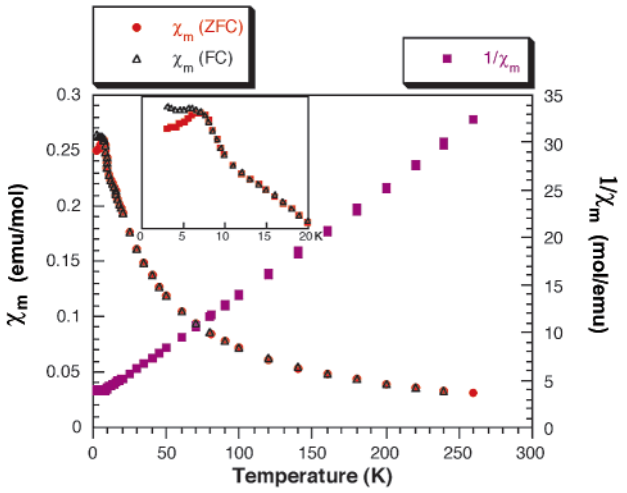

Figure 7. Isotropic magnetic susceptibility of a polycrystalline sample of $Gd_{1.33}Pt_3Al_7Si$. The inset shows a more detailed view of the low temperature χ_m vs *T* behavior.

Magnetic Susceptibility Studies. Because of the disorder present in these structures, and the anisotropic environment and triangular distribution of gadolinium ions, these compounds have the potential for interesting magnetic characteristics such as spin glass behavior. To investigate this possibility, magnetic susceptibility measurements were carried out on powdered samples and oriented crystals. The magnetic susceptibility data for a polycrystalline sample of $Gd_{1.3}Pt_3Al_7Si$ are shown in Figure 7. This compound exhibits Curie−Weiss behavior above 50 K; the magnetic moment/gadolinium atom derived from these data (8.3 μ_B) is in agreement with the theoretical value for free Gd^{3+} ions (7.94 μ_B). The high-temperature data for the ternary $Gd_{1.3}Pt_3Al_8$ and the $Gd_{0.67}Pt_2(Al,Si)_5$ compounds are similar. This indicates that platinum is diamagnetic in these materials, and it is consistent with the many examples of nonmagnetic late transition metals (TM's) in rare-earth containing interme-

(15) (a) Pechev, S.; Bobet, J. L.; Chevalier, B.; Darriet, B.; Weill, F. *J. Solid State Chem.* **2000**, *150*, 62−71. (b) Blazina, Z.; Sorgic, B.; Drasner, A. *J. Phys. Condens. Matter* **1999**, *11*, 3105−3114.
(16) Buschinger, B.; Geibel, C.; Weiden, M.; Dietrich, C.; Cordier, G.; Olesch, G.; Kohler, J.; Steglich, F. *J. Alloys Cmpd.* **1997**, *260*, 44−49.

tallics. The electronegativity of the metals in the Fe, Co, Ni, and Cu families (all >1.8 on the Pauling scale, with platinum at 2.2) is greater than that of aluminum (1.5) and silicon (1.8).[17] Thus, in ternary or quaternary materials RE/TM/Al-(Si), the electrons donated by the rare earth ions will likely be accepted to a large extent by the transition metal, filling up the d-orbitals and resulting in no magnetic moment on the TM atoms. Evidence of this has been seen in compounds such as $Gd_3Ni_6Al_2$,[18] $RERu_2Al_{10}$,[19] and $SmNiSi_3$.[3]

Antiferromagnetic ordering is indicated in the data for $Gd_{1.33}Pt_3Al_8$ by a cusp in the temperature dependence of χ_m at 20 K. This is consistent with the negative Weiss constant of −35 K derived from the inverse susceptibility fit. The data for the silicon containing quaternary compound are more complex, showing a discontinuity at 15−20 K (a slight dip) and a more pronounced antiferromagnetic cusp at 7 K. This could be an indication of local nanoscopic inhomogeneities in composition, with Si-rich regions of the sample alternating with Si-poor regions. The latter could behave much like the ternary $Gd_{1.33}Pt_3Al_8$ with an antiferromagnetic transition at 15 K. In Si-rich regions of the sample, the disorder is greater and therefore the exchange energy between the gadolinium ions is lower, resulting in the antiferromagnetic transition being shifted to lower temperature (7 K). Similar evidence of disorder hindering the magnetic interactions between rare earth ions has been observed in an investigation of the Laves phase $GdAl_2$ doped with a variety of nonmagnetic species to form a series of $Gd(Al_{1-x}M_x)_2$.[20] As the concentration of M increases, the Curie temperature of this compound decreased; it is noteworthy that the effect was most drastic for M = silicon. This correlated well with calculated changes in the value of the DOS at E_f as a dopant was added.

This doping effect is also apparent in the data for the $Gd_{0.67}Pt_2(Al,Si)_5$ compounds. As shown in Figure 8, the ternary compound $Gd_{0.67}Pt_2Al_5$ undergoes antiferromagnetic ordering at 8 K. For the silicon-containing analogue, no transition is seen down to 3 K, although fitting of the data shows a negative Weiss constant, indicative of an antiferromagnetic exchange interaction. It is interesting that even though $Gd_{0.67}Pt_2(Al,Si)_5$ contains the same disordered Gd/Al planes and Pt_2Al_4 layers as $Gd_{1.3}Pt_3(Al,Si)_8$, the magnetic ordering is shifted down to lower temperatures. This may indicate that the observed coupling in $Gd_{1.3}Pt_3(Al,Si)_8$ takes place across the $PtAl_2$ layers. This layer separates two Gd/Al layers at a distance of 5.5 Å, as opposed to the 8.3 Å distance across the Pt_2Al_4 moiety. However, proximity of the magnetic ions to one another is only one of the two main factors that control magnetic interactions in metallic compounds. In conducting materials, the conduction electrons mediate exchange between localized moments; the strength of the interaction is therefore dependent on the band structure

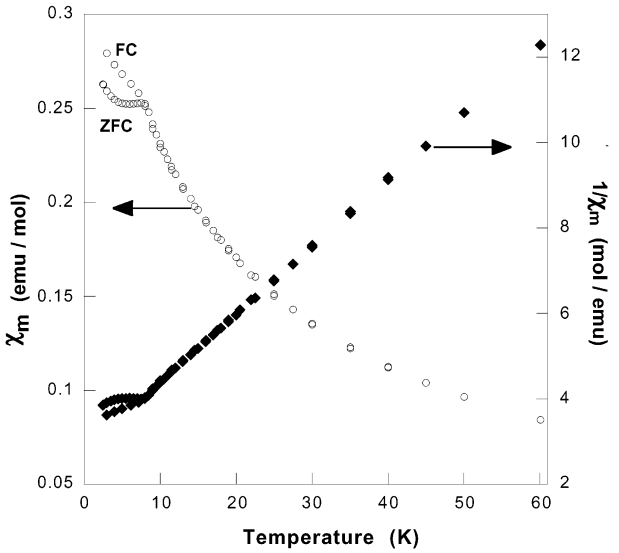

Figure 8. Isotropic magnetic susceptibility of a polycrystalline sample of $Gd_{0.67}Pt_2Al_5$. The field-cooled (FC) and zero-field-cooled (ZFC) susceptibility data are labeled.

at the Fermi level, as well as the distribution of spins.[21] It is not known how the DOS at E_f of these two structure types differ.

The magnetic behavior of $Gd_{0.67}Pt_2(Al,Si)_5$ and $Gd_{1.33}Pt_3(Al,Si)_8$ may be further complicated by the disorder in the Gd/Al layers. The superstructure model of the Gd/Al plane shown in Figure 4b indicates that each Gd has three nearest Gd neighbors at a distance of 4.3 Å. Even if each Gd/Al slab is thus ordered, the lack of superstructure peaks in the X-ray data indicates that the layers are not ordered with respect to each other. This has the potential to result in unusual magnetic phenomena. Evidence of this possibility is found in the divergence of the isotropic field-cooled (FC) and zero-field-cooled (ZFC) susceptibility, examples of which are seen in Figures 7 and 8. This FC−ZFC hysteresis behavior is often found in spin glass systems.[22]

Single-Crystal Magnetic Susceptibility Measurements. The anisotropic nature of the $Gd_{1.3}Pt_3(Al,Si)_8$ structure, with layers containing rare earth ions separated by nonmagnetic layers, is likely to produce strong orientation dependence in the magnetic behavior. Because the orientation of the layers was obvious from the crystal morphology, the directional dependence of the magnetic susceptibility was investigated. Figure 9 shows an expanded view of the anisotropic low-temperature data for both compounds. Theoretically, a material with localized electrons that order antiferromagnetically with their spins aligned along the magnetic field should show a precipitous drop in χ_m below the Neel temperature. If the spins are aligned along a direction perpendicular to the field, χ_m should level off as the temperature drops below T_N. If one looks at the data for $Gd_{1.3}Pt_3(Al,Si)_8$ as a function of crystal orientation, it is apparent that the spins are lying in the basal plane when ordered. The "parallel" and "perpendicular" descriptions in the legend of

(17) Lee, J. D. *Concise Inorganic Chemistry*; Chapman and Hall: London, 1991; p 160.
(18) Pechev, S.; Chevalier, B.; Khrussanova, M.; Terzieva, M.; Bobet, J. L.; Darriet, B.; Pechev, P. *J. Alloys Compd.* **1997**, *259*, 24.
(19) Szytula, A., Leciejewicz, J., Eds. *Handbook of Crystal Structures and Magnetic Properties of Rare Earth Intermetallics*; CRC Press: Boca Raton, FL, 1994.
(20) Magnitskaya, M.; Chelkowska, G.; Borstel, G.; Neumann, M.; Ufer, H. *J. Electron Spectrosc*. **1994**, *68*, 525−529.
(21) Kittel, C. *Solid State Phys.* **1968**, *22*, 1.
(22) Mydosh, J. A. *Spin Glasses: an experimental introduction*; Taylor & Francis: London, 1993.

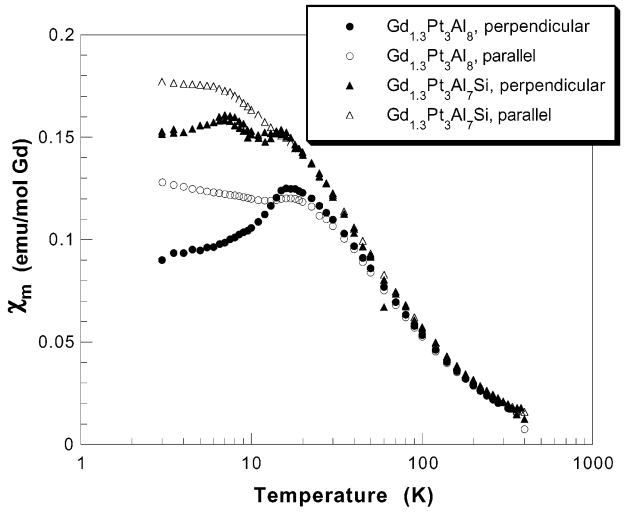

Figure 9. Magnetic susceptibility data for crystals of $Gd_{1.33}Pt_3Al_8$ and $Gd_{1.33}Pt_3Al_7Si$ oriented with their *c*-axes parallel and perpendicular to the magnetic field. A log scale is used for the temperature axis to emphasize the low-temperature region.

Figure 9 refer to the orientation of the *c*-axis with respect to the field. It is when the crystals are placed in the field with their *c*-axes perpendicular to the field that the drop in χ_m characteristic of spins aligned along the field of the magnet occurs. Conversely, when the *c*-axes of the crystals are aligned parallel to the field, a leveling off of χ_m is seen (the slight rise below T_N is due to the presence of a small amount of paramagnetic impurities).

Concluding Remarks

The combination of Gd, Pt, and Si in molten aluminum has resulted in the formation of compounds with two structure types containing similar structural motifs. In addition to stuffed arsenic-type $PtAl_2$ layers, both structure types also possess a Gd/Al triangle layer. The low reaction temperatures afforded by synthesis in aluminum flux has allowed for highly disordered positioning of these Gd/Al layers, in contrast to the ordered stacking of similar layers in other compounds synthesized by arc melting followed by annealing. $Gd_{1.33}Pt_3Al_7Si$ can be described as a pseudoternary disordered variant of $Gd_4Pt_9Al_{24}$; the same variant structure is also formed without silicon ($Gd_{1.33}Pt_3Al_8$). $Gd_{0.67}Pt_2Al_4Si$ and its ternary analogue are isostructural with $RE_{0.67}Ni_2Ga_{5-x}Ge_x$. A specific crystallographic site for silicon has not been located in either structure.

The antiferromagnetic coupling between the Gd^{3+} ions in $Gd_{1.33}Pt_3Al_8$, with a T_N of 20 K, is suppressed by the addition of silicon into the structure, lowering the ordering temperature to 7 K. Orientation dependence of the susceptibility indicates anisotropic exchange forces, in agreement with the layered nature of the structure.

Acknowledgment. Financial support from the Department of Energy (Grant DE-FG02-99ER45793) is gratefully acknowledged. This work made use of the SEM facilities of the Center for Electron Optics at Michigan State University. We thank B. Sieve, M. Zhuravleva, and S. D. Mahanti for useful discussions during the preparation of this manuscript.

Supporting Information Available: Additional X-ray crystallographic data such as anisotropic thermal parameters and complete tables of bond distances and angles for all four compounds are available in CIF format. This material is available free of charge via the Internet at http://pubs.acs.org.

IC025623N